Quantitative Autofluorescence and Cell Density Maps of the Human Retinal Pigment Epithelium

Thomas Ach,[1] Carrie Huisingh,[1] Gerald McGwin Jr,[1,2] Jeffrey D. Messinger,[1] Tianjiao Zhang,[1] Mark J. Bentley,[3] Danielle B. Gutierrez,[4] Zsolt Ablonczy,[5] R. Theodore Smith,[6] Kenneth R. Sloan,[3] and Christine A. Curcio[1]

[1]University of Alabama at Birmingham, Department of Ophthalmology, Birmingham, Alabama, United States
[2]University of Alabama at Birmingham, Department of Epidemiology, Birmingham, Alabama, United States
[3]University of Alabama at Birmingham, Department of Computer and Information Sciences, Birmingham, Alabama, United States
[4]Center for Coastal Studies, Texas A&M University-Corpus Christi, Corpus Christi, Texas, United States
[5]Medical University of South Carolina, Department of Ophthalmology, Charleston, South Carolina, United States
[6]New York University School of Medicine, Department of Ophthalmology, New York, New York, United States

PURPOSE. Lipofuscin (LF) accumulation within RPE cells is considered pathogenic in AMD. To test whether LF contributes to RPE cell loss in aging and to provide a cellular basis for fundus autofluorescence (AF) we created maps of human RPE cell number and histologic AF.

METHODS. Retinal pigment epithelium–Bruch's membrane flat mounts were prepared from 20 donor eyes ($10 \leq 51$ and $10 > 80$ years; postmortem: ≤ 4.2 hours; no retinal pathologies), preserving foveal position. Phalloidin-binding RPE cytoskeleton and LF-AF (488-nm excitation) were imaged at up to 90 predefined positions. Maps were assembled from 83,330 cells in 1470 locations. From Voronoi regions representing each cell, the number of neighbors, cell area, and total AF intensity normalized to an AF standard was determined.

RESULTS. Highly variable between individuals, RPE-AF increases significantly with age. A perifoveal ring of high AF mirrors rod photoreceptor topography and fundus-AF. Retinal pigment epithelium cell density peaks at the fovea, independent of age, yet no net RPE cell loss is detectable. The RPE monolayer undergoes considerable lifelong re-modeling. The relationship of cell size and AF, a surrogate for LF concentration, is orderly and linear in both groups. Autofluorescence topography differs distinctly from the topography of age-related rod loss.

CONCLUSIONS. Digital maps of quantitative AF, cell density, and packing geometry provide metrics for cellular-resolution clinical imaging and model systems. The uncoupling of RPE LF content, cell number, and photoreceptor topography in aging challenges LF's role in AMD.

Keywords: retinal pigment epithelium, autofluorescence, photoreceptor, lipofuscin, cytoskeleton

The leading cause of untreatable vision loss and legal blindness in industrialized countries is AMD, a disease of the photoreceptor support system, involving alterations of the RPE.[1-4] The RPE performs numerous functions essential to the choroid and the photoreceptors,[5] including phagocytosis of photoreceptor outer segments, absorption of excess light, processing of retinoids for phototransduction (visual cycle), maintenance of the blood–retina barrier, and secretion of growth factors, cytokines,[6] and lipoprotein particles.[7] Lipofuscin, nondegradable and brightly fluorescent organelles in the lysosomal compartment of the RPE accumulate due to a very slow turnover of ingested photoreceptor fragments.[8-11] Retinal pigment epithelium lipofuscin is comprised of mostly lipids and less than 2% proteins.[12] The principal fluorophores are *bis*-retinoids,[13,14] byproducts of the visual cycle that delivers retinoids to photoreceptors, with abundant A2E (n-retinylidene-n-retinyl ethanolamine) being the best understood. Noninvasive fundus autofluorescence (AF) imaging has been important in the clinical diagnosis and management of chorioretinal diseases for nearly 2 decades, with principal signals mainly from the RPE.[15,16]

Because the largest risk factor for AMD is aging, the fact that RPE lipofuscin was more abundant in human macula than periphery[8] led to an early hypothesis that lipofuscin accumulation was toxic and contributed to outer retinal cell death in aging and AMD.[15,16] Counts of photoreceptors and RPE from sections of human eyes apparently showing age-related loss of both cells were presented in support of this hypothesis.[15] An alternate view of lipofuscin arises from a 1978 study by Wing and colleagues[17] demonstrating that like the topography of photoreceptors in human eyes,[18,19] total AF peaked in the perifovea where rods were numerous and dipped in the fovea where only cones are found.[18] This topography suggested a role for lipofuscin in the physiology of vision that has not been explored.[10,20]

The lipofuscin toxicity hypothesis can be tested by quantifying RPE cell number and AF levels in donors of different ages, with the RPE population expected to decline as lipofuscin accumulated. Published studies do not reveal

consistent age-changes in RPE cell number,[21-23] and the one study that also assessed histologic AF did not account for the inhomogeneity of macular photoreceptors.[15] As determined in flat mounts for maximal accuracy, rods are preferentially vulnerable to aging over cones[18,19,24] and at locations closer to the fovea than can be explained by lipofuscin.[17,24,25] Using spatial variation and differential vulnerability to aging as a strong independent variables, herein, we determined simultaneous RPE cell number and total AF (summed intensity of all excited lipofuscin fluorophores) in an en face view with simultaneous melanosome screening in human donor eyes of two age groups. As in prior photoreceptor mapping studies, we used flat-mounted tissues, systematic sampling, and computer-controlled microscopy, and we developed new methods to reference RPE layer locations to the overlying retina in millimeters. These digital maps provide new human RPE metrics and little evidence that lipofuscin accumulation impacts negatively on RPE cell numbers or packing geometry.

METHODS

Tissue

Twenty eyes from 20 donors ($10 \leq 51$ years, $10 > 80$ years) were obtained from 1996 to 1999 from the Alabama Eye Bank within 4.2 hours of death (median: 2.3 hours; Supplementary Tables S1 and S2). The institutional review board at the University of Alabama at Birmingham approved the use of human tissue, which conformed to the guidelines of the Declaration of Helsinki. After cornea and iris were removed, the globe was preserved by immersion in 4% paraformaldehyde/0.1 M PBS for 24 hours. After removal of vitreous and sclera, chorioretinal tissue ($\sim$20- to 25-mm total width) including optic disc, macula, and the retinal vascular arcades was cut and cryoprotected in glycerol:Sorensen phosphate buffer (SPB, 0.1 M) solution and frozen ($-80°$C) until used. Tissue was thawed at 4°C overnight and rehydrated in successive glycerol:SPB solutions (40:60, 30:70, 20:80, 10:90, respectively; 24 hours in each) and stored in 100% SPB for 3 days. Before freezing, all maculas were determined to be grossly normal by inspection under a dissection microscope with trans- and oblique epi-illumination.[26] After freezing, ex vivo spectral domain optical coherence tomography and AF images (Spectralis, Heidelberg Engineering, Heidelberg, Germany) corroborated these assessments, for 15 tissues.

A2E Analysis by Mass Spectrometry

To determine if the used tissue preservation and storage methods affected major fluorophores of RPE-AF, the abundance of A2E was quantitated in recently collected and similarly prepared tissue punches from four eyes of two donors (63- and 67-year-old Caucasian females lacking retinopathy) following published methods.[27] One eye of each donor was fixed in 4% paraformaldehyde, and with the fellow eye was untreated. Six RPE/choroid punches (5-mm diameter) of macula (2) and periphery (4) were stored at $-80°$C for 1 month. A2E was extracted and reconstituted for analysis under dim red light and mass spectrometric analysis was performed on an Agilent 1200 HPLC in-line with an Agilent 6410 triple quadruple with an electrospray ionization source (Santa Clara, CA, USA).[27] Samples were analyzed using Agilent MassHunter Qualitative Analysis software, version B.03.01 in full-scan (mass-to-charge ratio [m/z] 100–1000) and multiple reaction monitoring modes. Transitions to the following product ions were monitored for the detection of A2E ([M+H]$^+$ 592.5): m/z 105.2 (quantifier ion), m/z 404.2, m/z 418.2. Results indicated

that our tissue preservation methods did not preclude detection of A2E (Supplementary Fig. S1), for this length of time in storage. Longer storage times may have influenced A2E detectability.

Preparing RPE-BrM-Flat Mounts

Using a dissection microscope (SMZ800, Nikon Instruments, Inc., Melville, NY, USA), we prepared RPE-BrM-flat mounts in a multistep, photodocumented (Supplementary Fig. S2), process (SMZ-U Zoom 1:10, Nikon Co-olpix P5000, Nikon, Japan;). (1) Retina-on: from the tissue belt a central 20×20–mm part including optic disc and macula was excised. To optimize tissue flatness for microscopy, the tissue was relaxed with several cuts, (2) retina-off: the retina was detached from the RPE using forceps (No. 7; WPI, Sarasota, FL, USA) to exclude light absorption by the luteal pigment of the neurosensory retina during AF imaging. In a few tissues, the retina tightly adhered to the RPE, which resulted in loss of small RPE patches, and (3) retina+choroid-off: choroid vessels were removed with forceps, membrane peeler, and spatula (G-37513; G-16189, Geuder, Heidelberg, Germany), and/or brushes (Camel 4 round; Tree House, Oklahoma City, OK, USA) in a SPB-filled dish. Complete removal of choroid for one specimen took 6 to 8 hours of fine preparation. The resulting RPE monolayer attached to BrM was approximately 20-µm thick. Previous studies of whole mounts have shown minimal shrinkage confined to the tissue edge.[19]

Phalloidin Labeling and Tissue Mounting

Single RPE cells were delineated using phalloidin labeling of filamentous actin (F-actin) to display the cytoskeleton and cell shapes in en face imaging.[28] Tissues were extracted with 0.1% Triton X-100 (#11332481001; Roche, Mannheim, Germany) for 3 minutes and rinsed (3×5 minutes) with SPB. Each flat mount was labeled with Alexa Fluor 647 phalloidin (final concentration: 3 units/µL, #A22287; Life Technologies, Grand Island, NY, USA) for 20 minutes at room temperature and rinsed (three times for 5 minutes each) with SPB.

Tissues were mounted as flat as possible with BrM down on microscope slides (#12-550-15; Fisher Scientific, Pittsburgh, PA, USA). Remaining fluid beneath the tissue was absorbed with surgical wedge sponges (Sugi; Kettenbach, Eschenbach, Germany) before mounting (#P36930, ProLong Gold antifade reagent; Molecular Probes, Eugene, OR, USA) and cover slipping (#061812-9; Fisher Scientific). Exposure to light was minimized. Slides were stored in the dark.

Preserving Foveal Position

To generate AF and cell density maps on a common fovea-centered coordinate system, it is crucial to have at least one common landmark in all tissues. We carefully maintain consistent orientation, placing the optic disc on the horizontal axis. Using a custom written ImageJ software plugin (http://imagej.nih.gov/ij/; provided in the public domain by the National Institutes of Health, Bethesda, MD, USA), an image overlay showing landmarks common to each dissection step specified the exact location of the fovea (Fig. 1). Starting with the retina on-image, the fovea was localized to a characteristic dip and a reddish, darker spot due to light reflecting from the choroid and passing through thin overlying tissue. Two to four landmarks (tissue cuts, choroidal vessel crossings, pigmentation) on the retina-off and retina+choroid-off images were used by custom software to register each image to the previous one. Finally, an image overview of the mounted tissue was acquired using a microscope (see below). Common landmarks between
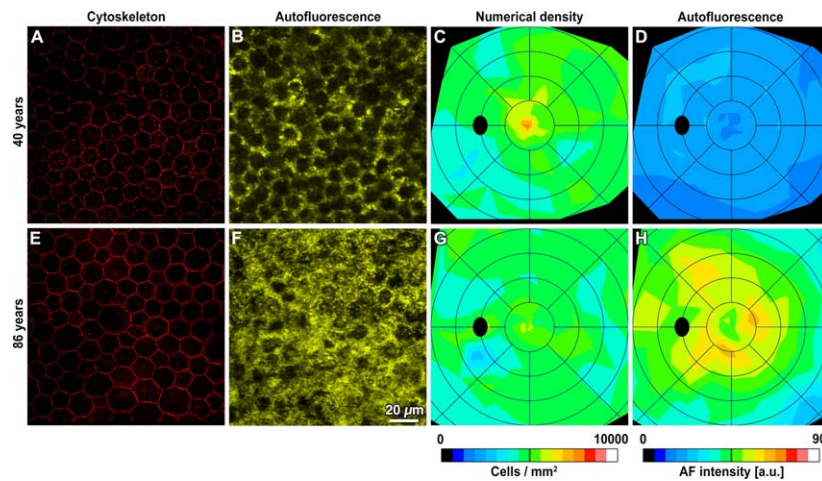
FIGURE 1. Retinal pigment epithelium–BrM flat-mount cytoskeleton and AF images are the basis for numerical density and AF maps. Representative micrographs and digital maps show two donors at different ages. For each map, RPE flat mounts were imaged at 75 to 90 predefined locations in an unbiased sampling pattern (Supplementary Table S2). At each location, cytoskeleton imaging ([**A**, **E**] fovea is shown) was followed by lipofuscin AF imaging (**B**, **F**). Single RPE cells are delimited by labeled cytoskeleton (**A**, **E**). Autofluorescence values were normalized by a reference standard.[34] The RPE layer shows variable AF (**B**, **F**), because the lipofuscin load differs from cell to cell, and because other organelles occupy space and block signal transmission (e.g., nuclei in the middle and melanosomes in the apical 1/3). Retinal pigment epithelium numerical density (**C**, **G**) peaks in the foveal center, decreases with eccentricity, and is similar in these age groups. Autofluorescence intensity (**D**, **H**) is highest outside the foveal center in a perifoveal annulus and is higher in the older eye. Maps are displayed as left eyes, and rings are centered on the fovea and at intervals of 2 mm. The black oval represents the optic disk. Maps of all study eyes are presented in Supplementary Figures S4 and S5.

this final image and the retina+choroid-off image projected the fovea onto the RPE-BrM-flat mount.

Sampling Scheme

We used a systematic and unbiased sampling scheme to include RPE in areas with distinctive levels of photoreceptor related metabolism (fovea: cones only; perifovea: highest rod density; near periphery: highest rod cone ratio). Samples were more closely spaced where gradients in cell density were expected.[23,29] Imaging (see below) was performed at eight evenly spaced positions on rings with increasing diameter centered around the fovea (radii for the three inner circles: 0.2 mm, 0.5 mm, and 1 mm; radius ring(i) (4 and higher) = (i-2) × 1.0 mm), creating an even tessellation of the tissue (Supplementary Fig. S3). A total of 75 to 90 areas per tissue were imaged, depending on variations in tissue size and tissue integrity (Supplementary Table S3).

Imaging

Fluorescence imaging used a BX51 microscope (Olympus, Center Valley, PA, USA) with a motorized stage control, oil objective (UPlanApo ×40 oil iris, numerical aperture 1.0; Olympus), digital camera (Orca R^2, Hamamatsu, Middlesex, NJ, USA), excitation light source emitting a mercury arc lamp spectrum (Xcite 120Q, Lumen Dynamics Group Inc., Mississauga, Ontario, Canada), and filter cubes for cytoskeleton imaging (LF635-B-000, excitation 635 nm, emission >650 nm; Semrock Inc., Rochester, NY, USA) and AF lipofuscin imaging (Long-pass GFP filter cube OSF-GFP-30LP-B-Z, excitation: 460–490 nm, emission >505 nm, Semrock Inc.), all under control of the integrated microscope software (cellSens Dimension V1.7.1; Olympus). Camera parameters were set to: CCD sensitivity HighLight mode, pixel clock 28 MHz, resolution 1344 × 1024 pixels.

To capture the RPE cytoskeleton, tissue was scanned in several micrometers in the z-direction (in 0.4-mm steps). The exposure time for AF imaging was determined on trial basis from 2 to 3 perifoveal regions where high AF signal was

expected.[30] Exposure times were adjusted so that the maximum pixel intensity fell within the linear range of the fluorescence reference intensity. Scans in z-direction through the RPE cells were acquired in an apical to basal direction. Granules at the beginning of the range were back-focused 2 μm to ensure full capture of the entire cell. Potential loss of signal due to scattering of light passing through the tissue was not further evaluated. The effect of fluorophore quenching was tested using the same settings used for AF imaging. Two RPE-BrM tissues were excited continuously over 15 minutes, and images were taken every 30 seconds. Within the first minute, AF intensity decreased approximately 10%. During follow-up, AF further decreased (down to 70% of the original AF), with a steady state after approximately 5 minutes. Since our AF measurements at one location were performed in significantly less than 1 minute (~25 seconds), fluorescence quenching could be omitted from the AF analysis.

Image Postprocessing

All images were processed using the microscope software. Cytoskeleton imaging was followed by a 3-dimensional deconvolution for every frame of the z-stack using the constrained iterative module with the advanced maximum likelihood estimation algorithm (ADVMLE, 10 iterations). The extended focal imaging (EFI) module generated a projection image from the z-stack. Signal originating from labeled f-actin within RPE apical processes was removed with the "background subtraction" tool. Background was reduced to get clearly delineated cytoskeletons. Imaging of autofluorescent granules was followed by EFI processing only, without background subtraction.

Cell Counts, Voronoi Analysis (Supplementary Fig. S3)

We used images of phalloidin-labeled RPE to define the center of each cell using a custom ImageJ plugin. In many images, these estimates required examination and only minor editing by a trained observer. In others, cell centers were identified

manually. For accurate cell densities, we defined a central counting window in each image. This manually-chosen polygon had at least one row of cells between it and the image edge, and it included only cells with clearly delimited cytoskeletons. Delaunay triangulation and Voronoi Diagrams are well-established methods in retinal neurobiology in defining plane cellular mosaics.[31-33] Voronoi Diagrams were generated for every RPE cytoskeleton image for determining RPE packing geometry and cell area. A Voronoi Diagram is a collection of regions that tessellate a plane, appearing similar but not identical to an image of the cells. Voronoi regions were used as surrogates for cells. The Delaunay triangulation is the "straight line dual" of the Voronoi Diagram and provided information about packing geometry. Autofluorescence for each cell was computed by summing intensities for all pixels whose centers were inside the Voronoi region containing that cell's center. Autofluorescence for the entire image was computed from the individual cell values. All AF values were normalized to a common standard (see below).

Maps of Derived Values

Composite maps of mean cell density and AF between age groups and differences between age groups were computed for points assigned to nominal positions in the standard sampling pattern,[24] despite minor positional variations between tissues. Differences between 51 years and younger and older than 80 years of age groups were computed for all possible pairs of younger and older eyes at each sample point, and the mean of those differences was calculated. For display, values at locations between the nominal sampling points were linearly interpolated.

Fluorescence Reference Standard

Properties of the fluorescence reference are detailed elsewhere.[34] Texas red dye and other proprietary compounds are embedded in a plastic matrix (Microscopy/Microscopy Education, McKinney, TX, USA). The reference was examined to verify that the distribution of fluorescent material within it was homogeneous by examining five randomly-chosen images taken on two different days (data not shown).

Normalization of AF

AF intensities were normalized using these formulas:

$$I_R = (G \times \tau_R \times R) \tag{1}$$

$$I_{AF} = (G \times \tau_{AF} \times AF) \tag{2}$$

$$R = I_R/(G \times \tau_R) \tag{3}$$

$$AF = I_{AF}/(G \times \tau_{AF}) \tag{4}$$

$$AF/R = (I_{AF} \times \tau_R)/(I_R \times \tau_{AF}) \tag{5}$$

where G = gain of detection system (including optics and filters); R = fluorescence emission from reference; AF = fluorescence emission from retina; I_R = measured reference signal integrated over the exposure duration τ_R; I_{AF} = measured flat mount signal integrated over the exposure duration τ_{AF}.

Equations 1 through 3 are calculations of the fluorescence intensity of the reference; 4 is the calculation of the fluorescence intensity of the AF image; and 5 is the normalization formula for AF images at each location.

Plotting AF Versus Cell Area

For Voronoi regions representing individual RPE cells, total AF (intensities summed over all pixels within the RPE cytoskeleton) was plotted versus cell area.

If AF_{px} equals AF for one pixel (the sum of pixel intensities of a vertical stack of scans through the RPE cell), and N equals number of pixels within the RPE cytoskeleton boundary, then the total AF from one RPE cell is:

$$AF_{RPEcell} = \sum_{1}^{N} AF_{px} \tag{6}$$

$\frac{AF_{RPEcell}}{CellArea}$ is a projected concentration, since it reflects the sum of all pixels in the volume of the RPE cell.

There are limitations to this analysis. For our plots, we assumed a linear relationship between total AF per cell and cell area. We also determined that R^2 of linear and quadratic regressions did not provide better fits (data not shown).

Statistical Analysis

Linear regression mixed models were used to assess the relationship between age group with measured outcomes including cell density, AF, cell area, and number of neighbors for specified regions of the flat mounts. Mixed models were used to account for the within-person correlation that occurs when multiple observations are taken from the same specimen. The standard variance component covariance structure was specified. Similar models were used to assess the relationship between fovea and annulus categories with measured outcomes.

Analysis of covariance models were used to evaluate the relationship between age group and normalized AF after controlling for the area of individual cells. Two types of SEs are available for these models: empirical- and model-based estimators. Empirical- than model-based SEs were used, because they are based on actual variations in the cluster-level statistics, are considered to be more robust, and generate consistent estimates even with a nonspecific correlation structure.[35,36] After an iterative fitting process, an unstructured working correlation matrix was specified, because it minimized the difference in variance estimates between empirical and model-based SEs. Separate models were run for each region of the eye. An interaction term was included in the model to assess if the association between cell area and normalized AF differed by age group. PROC GENMOD in SAS v9.3 (SAS Institute, Inc., Cary, NC, USA) was used to account for within-specimen variance. For both models, _P_-values less than 0.05 were considered significant.

RESULTS

Overall topography of normalized RPE-AF and between-individual variability are shown for representative tissues (Figs. 1, 2; Supplementary Fig. S4). The highest AF eyes were in the older than 80 group (Supplementary Fig. S4). In both young and older eyes, AF was highest in a perifoveal annulus 2 to 4 mm from the fovea (Figs. 1D, 1H), patterns highlighted in composite maps of each age group (Figs. 2B, 2D). The topography of AF is strikingly similar to the topography of rod photoreceptors, which are absent from the foveal center and high in a perifoveal annulus that is horizontally elongated (Supplementary Fig. S6).[24,37] Interestingly, cones also contributed to AF signal, as the signal in the foveal rod-free zone was nonzero (Supplementary Fig. S4). Relative to AF, RPE cell density was less variable. The peak density of 7500 cells/mm²

was found at the fovea in both age groups, and density decreased gradually with eccentricity to values of approximately 5000 cells/mm² at the edge of the macula (3 mm; Figs. 1, 2; Supplementary Fig. S5; Supplementary Table S4). These densities are in agreement with previous studies reporting densities along single meridians (Fig. 2, Supplementary Table S2)[23,29] and are substantially higher than values reported for RPE flat mounts by investigators who also reported unusually low photoreceptor densities.[38] Accordingly, foveal RPE cells were significantly smaller than perifoveal and peripheral cells (Supplementary Table S4).[39,40]

Age groups were compared through difference maps. Despite individual variability, AF intensity increased significantly with age (Fig. 2; Supplementary Table S4), most prominently in an annulus of high AF but also extending superior-nasally, and at lower overall levels in the foveal center. In marked contrast, the RPE difference maps showed no significant cell loss with age (Fig. 2, Supplementary Table S4), and even a slight rise in some areas. Accordingly, the mean area of individual cells did not change significantly with age. Our observations concurred with previous literature showing minimal age-changes in density (Supplementary Table S3). Thus, high perifoveal AF in aging was unaccompanied by detectable changes in cell number.

Measures of spatial density may have masked small or focal losses that are accompanied by compensatory re-arrangements within the monolayer.[41] Therefore, we turned to a more sensitive measure of packing geometry, using Voronoi analysis to determine cell area and number of neighbors.[33] Maximum and minimum cell areas were more variable in older eyes than younger eyes (Supplementary Table S4). The energetically most favorable state for RPE cells is hexagonal,[40,42] with constant center-to-center spacing and six neighbors.[43] We found a predominance of six-neighbored cells only in the younger adult fovea, where 58.9% of cells had six neighbors (Fig. 3). In older eyes, smaller cells had three to four neighbors, and larger cells had eight or more neighbors, up to 13 (Fig. 3). With age, the proportion of six-neighbored RPE cells decreased, and six-nonneighbored cells increased, with a significantly higher proportion of cells with greater than or equal to eight neighbors (Fig. 3). Thus, we conclude that RPE cells continuously re-arrange themselves during lifetime, including in younger adults. That lipofuscin load initiates this re-arrangement seems unlikely in that this process occurs similarly in all regions examined. While not appreciably losing cells, the intact RPE monolayer nevertheless dynamically responds to its environment and maintains geometric precision.

It is also possible that measures of mean AF masks age-related changes in the fluorescence of individual RPE cells with potential significance for cell loss at more extreme ages or in AMD. For example, unusually bright cells with a high lipofuscin load may be particularly vulnerable to disease. It was apparent that the AF of individual cells was highly variable in each of three canonical retinal locations of older eyes (Supplementary Table S5), with a coefficient of variation (SD/mean) of approximately 80%. This variability was explored by assessing the relationship of AF to cell area, with ΔAF/ Δarea (slope of a linear fit) serving as a surrogate for the cellular concentration of lipofuscin. This analysis revealed that the total AF of an individual cell increased with cell size (Fig. 4), most likely due to more intracellular AF granules, fewer light-blocking melanosomes, or both.[8,9] Similar linear fits were found across ages at the fovea and perifovea (Fig. 4). In the periphery of older eyes, this relationship had steep slopes. This may be explained in part by reduced screening by melanosomes. It also cannot be excluded that our peripheral samples, at 8- to 10-mm eccentricity, were approaching the retinal edge where fluorophore A2E is abundant in humans
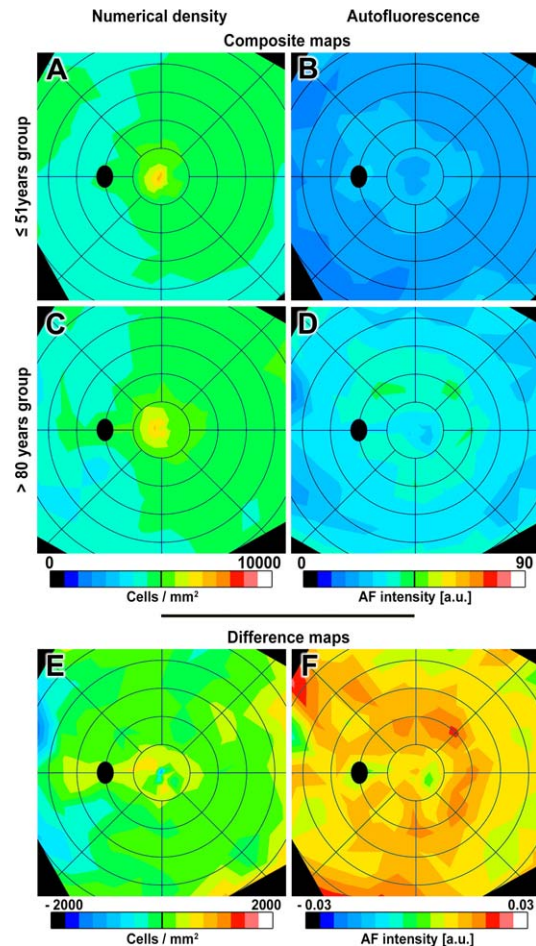

FIGURE 2. Composite and difference maps of RPE numerical density and AF. Composite and difference maps of numerical density and AF (AF intensity of human RPE in individuals ≤ 51 years and > 80 years). Composite maps (**A–D**): RPE numerical density peaks at the fovea (≤ 51: 6520 ± 946 cells/mm²; >80: 6405 ± 1323 cells/mm²) and decreases with eccentricity in both age groups (Supplementary Table S4). An annulus of intense AF localizes to the perifovea in both age groups, corresponding to highest rod densities (Supplementary Fig. S6) but slightly lower in inferior nasal quadrant.[83] Difference maps (**E–F**): *warm colors* indicate higher values, and *cool colors* indicate lower values in the older group. *Green* indicates minimal differences between groups. The numerical density difference map shows no significant age change at fovea and periphery and a significant increase in cell density with age in the perifovea (details in Supplementary Table S4). The AF difference map shows significantly increased intensity in all regions with age, especially at 2 to 4 mm from the foveal center. Difference maps display the mean of all pair-wise differences between eyes each of the locations analyzed in flat mounts. Excluding the youngest donor (16 years) from the analysis did not change the results. *Color bar* for differences in numerical density ranges between −2000 and +2000 cells in increments of 250 cells/mm². *Color bar* for differences in AF intensity ranges between −0.3 and +0.3 in increments of 0.0375 arbitrary units (a.u.). Other visualization conventions are the same as in Figure 1.

(Supplementary Fig. S1).[44] These data imply that lipofuscin load is regulated, and that regulatory principles are similar throughout adulthood in healthy eyes.

DISCUSSION

We provided the first maps of human RPE cell number and AF, without screening by pigments in overlying neurosensory
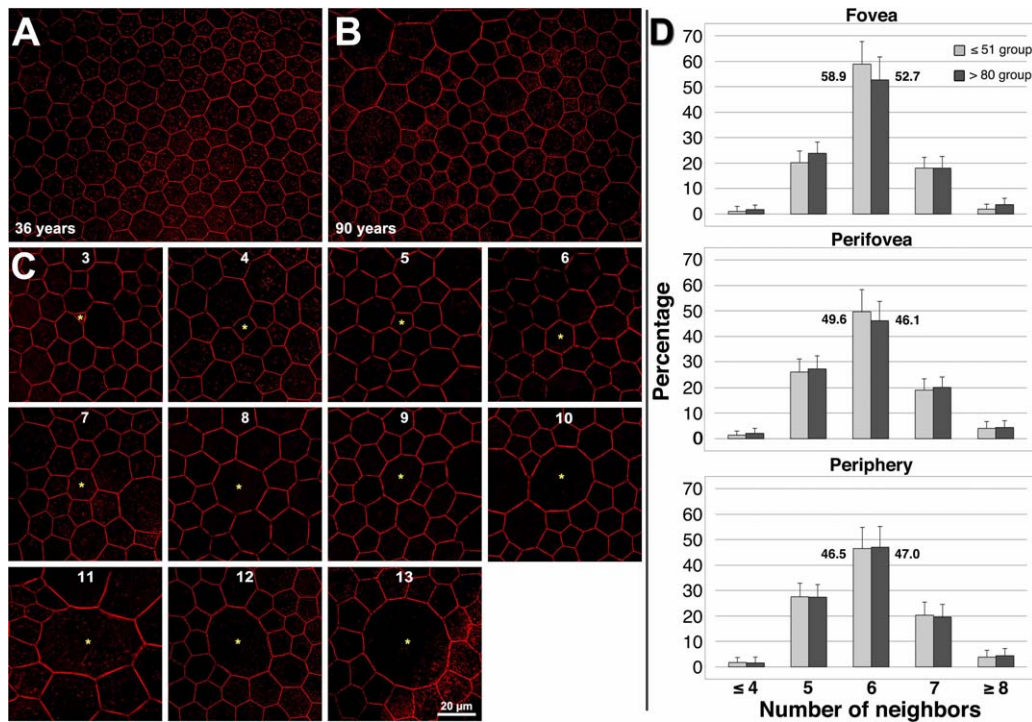
FIGURE 3. Retinal pigment epithelium cell packing geometry reflects monolayer remodeling over the lifespan. (**A, B**) Perifoveal RPE cells in a younger adult are mostly hexagonal in shape, with six neighbors, whereas cells in an older adult, while still polygonal, have a more variable number of neighbors. (**A**) A 36-year-old male donor, perifovea; (**B**) A 90-year-old female donor, perifovea. For illustrative purposes, *red* was manually sharpened and brightened in (**A, B**) using Photoshop CS6 (Adobe, San Jose, CA, USA). (**C**) Retinal pigment epithelium cells have 3 to 13 neighbors. Cells deviant from six neighbors can be found in both age groups. Phalloidin-labeling of actin cytoskeleton is shown. (**D**) Hexagonal cells are most frequent (>50%) in the fovea, and decrease in frequency (<50%) with increasing eccentricity from the fovea, confirming in vivo findings in humans by Morgan and colleagues.[33] With age, the number of cells with six neighbors decreases significantly in the fovea and perifovea. In contrast, in the fovea, the number of cells with five neighbors increases significantly, while in the perifovea the number of cells with five and seven neighbors increases significantly. Cell density, mean cell area, and number of neighbors (Supplementary Table S4) indicate RPE cell re-arrangement occurs throughout life (Supplementary Table S3). To highlight the differences in six-neighbored cells, the exact percentages are plotted next to the columns.
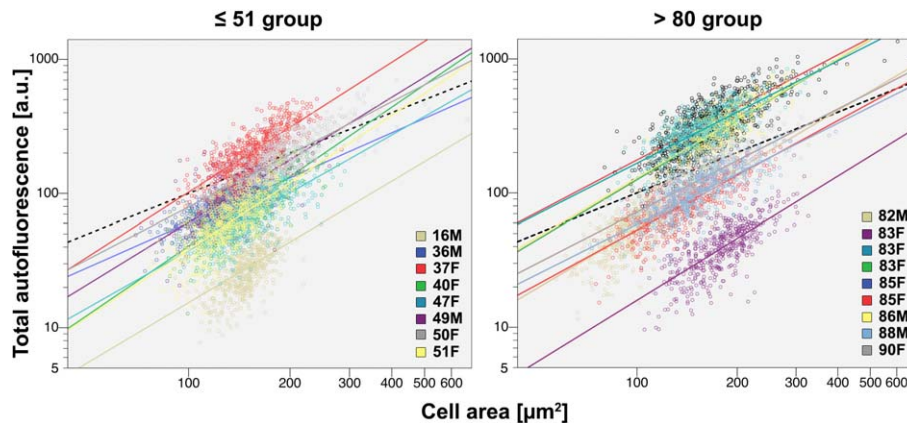

FIGURE 4. The relationship between total AF and cell area is a measure of lipofuscin concentration and how it is regulated. Total AF per cell increases with increasing cell size in both age groups. The slopes (ΔAF/Δcell area) do not change significantly with age at the fovea and perifovea (fovea: $P = 0.5662$, perifovea: $P = 0.5299$). Slopes are significantly steeper in the periphery ($P < 0.0001$) for the younger than 80-years group. This could be explained by more densely packed AF granules or loss of light blocking melanosomes[8] or, most likely, the recent observation that concentration of A2E, an abundant lipofuscin fluorophore, rises toward the retinal edge, where it is maximal.[44] The relationship ΔAF/Δcell area is a measure of the concentration of lipofuscin-attributable AF in individual cells. The plot shows total AF (a.u.) per cell versus cell area (μm^2) on a double logarithmic scale for illustrative clarity, for both age groups. Fovea, a region representative of other locations (for this measure, is shown (Supplementary Table S5). Total AF is the sum of AF intensities of all pixels bounded by cytoskeleton of an individual RPE cell. Autofluorescent granules within RPE cells are stacked rather than lying in a plane.[8] Therefore, AF is expressed as a planimetric density (Supplementary Fig. S3). Each circle represents a single cell. In total, more than 83,300 cells were analyzed (Supplementary Table S2). Linear fits are plotted for every tissue. Foveal data were not available from all 20 tissues.

retina but with screening of RPE melanosomes in an en face view, replicating the in vivo situation. Our results confirm and extend the results that Wing et al.,[17] obtained in histologic cross-sections in 1978 using a different eye donor pool (Boston versus Birmingham, unspecified race versus Caucasian). Because our maps accounted for macular photoreceptor inhomogeneity, our results reinforce the concept that RPE lipofuscin formation starts at the photoreceptor outer segments[13] and suggest that the topography of lipofuscin may reflect differences in phagosome production and/or processing by RPE in rod- and cone-rich areas of the macula. This idea was considered early[10,17] but was downplayed in pursuit of lipofuscin toxicity and macular pigment protection theories, and on the basis of evidence from animal models lacking strong gradients in photoreceptor topography.[20] Our novel analysis provided unique insights with multiple areas of high significance to clinical ocular imaging, diagnosis, and treatment.

First, our histologic AF maps provide a new cellular basis for clinical AF findings.[30,34,45] The variability, topography, and age-related increase in histologic RPE AF paralleled clinical qAF, which includes a photoreceptor bleaching step to isolate the RPE signal.[45] Consistent with the highest qAF intensities, peak histologic AF was found at an eccentricity of 10° to 15° (2.9–4.3 mm, perifovea) from the foveal center. Our results also reflect the clinically observed increase of the total fundus AF in healthy, aging maculas. As clinical qAF intensities decline after age 70,[30] our data from donors aged older than 80 years possibly reflects a somewhat decreased total fluorescence compared with the overall lifetime peak. Nevertheless, our histologic data appear to exclude cell loss as an explanation for the late life decrease in fundus AF. Other explanations for this decline, such as an age-related increase in screening by melanosomes or a dramatic reduction in photoreceptor outer segment length, seem also unlikely.[9,46] In particular, the consistency of our results with AF in flat mounts and with AF in tissue sections,[17] which largely obviates concern about screening by melanosomes, suggest that melanosome reduction is not responsible for these results. Therefore, we hypothesize that this decrease is due to the loss of lipofuscin granules from individual RPE cells, signifying declining health. Conversely, the rise in RPE-AF in vivo before 70 years is not detrimental and may be neutral in its effect, at least on cell number. The effect of lipofuscin on other RPE functions in vivo remains undetermined but may be neutral also.

Second, our data indicate that a contribution of RPE lipofuscin to the age-related loss of overlying rod photoreceptors is unlikely. An early histologic analysis that permitted neither accurate counts nor accurate localization relative to the fovea reported loss of photoreceptors and RPE, correlated with RPE lipofuscin.[15] In contrast our studies using whole-mounted retinas concluded that the primary locus of macular rod loss was close to the fovea (0.5- to 3-mm eccentricity), that is, on the inner slope of the ring of highest lipofuscin accumulation (Fig. 5).[24,25] Further, the current study found that foveal AF increased where cone photoreceptors were relatively stable in number. Thus, rod loss may be alternatively explained better by age-related changes elsewhere in the photoreceptor support system. With aging, Bruch's membrane, a vessel wall between the RPE and the choroidal blood supply, accumulates lipoproteins of intraocular origin,[47] creating a barrier to transport,[48] especially under the fovea, which lacks a blood supply from the inner retina. In this vascular insufficiency/nutritional deficiency model of aging,[49] rods are affected before RPE, because they are further from the vasculature, and before cones, because cones are additionally supported by Müller cells, at least for retinoids. Over time, translocation of essential nutrients to the photoreceptors is hindered, causing their decline. Age-related choroidal thinning, choriocapillary
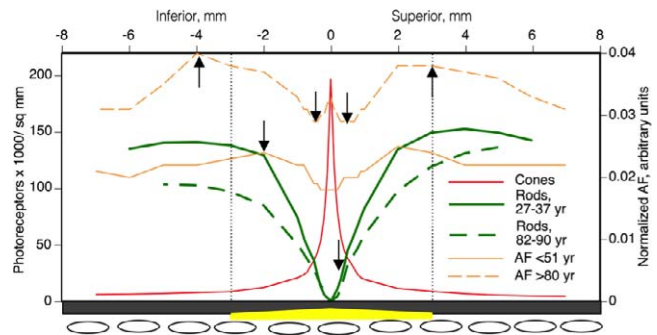

Figure 5. The topographies of age-related RPE-AF increase and photoreceptor loss in aging human retina are not obviously related.[24,25] Normalized AF along the vertical meridian from the 51 years or younger and the 80 years or older groups in the current study and spatial density photoreceptors along the same meridian from youngest adult group in Curcio et al.[24] are shown. Cone density was not shown to change with aging in the 1993 study and is illustrated for the oldest group only. *Dotted line* delimits the macula. The RPE-BrM-choriocapillaris complex is depicted schematically on the lower *x*-axis. An age-related accumulation in lipoproteins in BrM, believed to contribute to a transport barrier between choroidal vasculature and outer retinal cells,[48,84] and is thickest under the fovea (*yellow*).[85] *Arrows* indicate the highest proportional change for rod density and RPE-AF. Retinal pigment epithelium–AF increases most near the perifoveal rod ring and the foveal cone peak. Rod loss is worst where cone density is stable, and where an accumulation in BrM that would affect transport to both photoreceptor types is also abundant (*yellow*).

endothelial loss, and endothelial gene expression changes also support this model.[50,51]

Third, Voronoi analysis, a sensitive metric of cell packing in a monolayer, provided evidence that RPE undergoes a life-long re-arrangement. Possible mechanisms include cell division, compensatory enlargement after cell loss,[52] and fusion of neighboring cells. Unequal cell division[53] resulting in 3- and 13-neighbored cells is a possibility but human RPE cells[54] reportedly do not proliferate.[55] It is yet uncertain whether limited repair and regeneration arising from mitotic stem or progenitor cells[55] occurs in the postmitotic RPE. Interestingly, large RPE cells with more than six neighbors were polygonal, fit in an orderly mosaic, and obeyed population rules for fluorophore accumulation (Fig. 4), suggesting that they are healthy.[42] We observed multinucleate RPE cells,[39,56] implicating cell fusion, perhaps on a cooperative basis, as a strong candidate mechanism for producing large cells. Our data from elegant, polygonal, and spatially organized packing geometry of human RPE provides metrics for model systems. While cultured RPE cells may express RPE-specific proteins, their packing often differs qualitatively from that of native RPE. Therefore, an intact and polygonal (but not necessarily hexagonal) RPE cytoskeleton should be included as a criterion for physiological relevance of RPE and RPE-substitutes in culture. We hypothesize that deviation from this geometrically precise RPE polygonality potentially signifies distress, with an aberrant deployment of proteins leading to interpretable changes in morphology.

Fourth, our data bring from human eye pathology important new information to the debate on lipofuscin's role in AMD. The lipofuscin toxicity hypothesis has driven extensive research using cell culture, animal models, and clinical studies for 25 years. Unlike lipofuscin from other postmitotic cells which contains abundant proteins of mitochondrial origin,[57,58] the composition of RPE lipofuscin granules is uniquely *bis*-retinoid enriched.[12,59,60] A biosynthetic pathway starting with all-*trans* retinal in photoreceptors has been elucidated.[61] The most abundant *bis*-retinoid, A2E, was used in many in vitro

experiments that seemingly supported this hypothesis by achieving milestones of AMD progression-like cell death and complement activation, following exogenous loading and light exposure.[62] Hyper-AF at the border of geographic atrophy, an AMD end-stage featuring an inexorable spreading outward of RPE atrophy, superficially supported a mechanism of increased lipofuscin accumulation within individual cells before they succumbed.[63] These studies lead to the idea that reducing lipofuscin accumulation or detoxifying lipofuscin components are viable therapeutic strategies for GA, currently implemented in clinical trials and preclinical studies.[64-68] Moreover, the rationale for blue-blocking IOL implantation after cataract surgery for AMD prevention, which accounts for 25% of IOL worldwide,[69] assumes that lipofuscin components are photo-sensitizers.[70]

However, mounting evidence, including the current study, supports an alternate scenario. First, in the AMD end-stage of geographic atrophy, lipofuscin-attributable hyper-AF does not spatially predict progression,[71] and focal fundus hyper-AF can be just as easily explained by stacked cells as increased intracellular lipofuscin concentration.[72] Second, AF in the posterior pole is not primarily associated with A2E in situ in humans, although it is in mice.[44,73,74] Third, RPE with impaired autophagy recycles retinoids to photoreceptors poorly, suggesting that lipofuscin may even be necessary for healthy vision.[75] Fourth, alternate theories for cell death and extracellular lesion formation not involving lipofuscin, also based on new eye pathology findings, now exist.[76,77] Therefore, a critical evaluation of the lipofuscin toxicity hypothesis should be part of interpreting the outcomes of interventions involving visual cycle modulators[68] and blue-blocking IOL cataract surgeries.

Finally, quantitative descriptors of single RPE cells at precisely defined locations in human eyes will help validate advanced RPE diagnostic techniques just as accurate photoreceptor maps contributed to the development of adaptive optics-assisted cone imaging and rapid dark adaptometry, now available commercially.[78,79] These techniques include clinical qAF, adaptive optics scanning laser ophthalmoscopy linked to fluorescence or dark-field imaging,[80,81] and hyperspectral imaging to apportion total RPE-AF into constituent molecular peaks.[82] Our flat-mount data show RPE cell number, packing geometry, and AF as a snapshot in time, and it cannot be excluded that some of these donors might have developed AMD had they lived longer. This requisite limitation of histology will be addressed by our ongoing studies that investigate flat mounts of donors with AMD, and by longitudinal studies of living patients using imaging technologies newly informed by the normative data that we provide herein.

Disclosure: **T. Ach**, None; **C. Huisingh**, None; **G. McGwin Jr**, None; **J.D. Messinger**, None; **T. Zhang**, None; **M.J. Bentley**, None; **D.B. Gutierrez**, None; **Z. Ablonczy**, None; **R.T. Smith**, None; **K.R. Sloan**, None; **C.A. Curcio**, None

References

1. Ferris FL, Fine SL, Hyman L. Age-related macular degeneration and blindness due to neovascular maculopathy. *Arch Ophthalmol*. 1984;102:1640–1642.

2. Vingerling JR, Dielemans I, Hofman A, et al. The prevalence of age-related macuolpathy in the Rotterdam study. *Ophthalmology*. 1995;102:205–210.

3. Friedman DS, O'colmain BJ, Munoz B, et al. Prevalence of age-related macular degeneration in the United States. *Arch Ophthalmol*. 2004;122:564–572.

4. Williams RA, Brody BL, Thomas RG, Kaplan RM, Brown SI. The psychosocial impact of macular degeneration. *Arch Ophthalmol*. 1998;116:514–520.

5. Strauss O. The retinal pigment epithelium in visual function. *Physiol Rev*. 2005;85:845–881.

6. Shi G, Maminishkis A, Banzon T, et al. Control of chemokine gradients by the retinal pigment epithelium. *Invest Ophthalmol Vis Sci*. 2008;49:4620–4630.

7. Wang L, Li CM, Rudolf M, et al. Lipoprotein particles of intraocular origin in human Bruch membrane: an unusual lipid profile. *Invest Ophthalmol Vis Sci*. 2009;50:870–877.

8. Feeney L. Lipofuscin and melanin of human retinal pigment epithelium. Fluorescence, enzyme cytochemical, and ultra-structural studies. *Invest Ophthalmol Vis Sci*. 1978;17:583–600.

9. Feeney-Burns L, Hilderbrand ES, Eldridge S. Aging human RPE: morphometric analysis of macular, equatorial, and peripheral cells. *Invest Ophthalmol Vis Sci*. 1984;25:195–200.

10. Weiter JJ, Delori FC, Wing GL, Fitch KA. Retinal pigment epithelial lipofuscin and melanin and choroidal melanin in human eyes. *Invest Ophthalmol Vis Sci*. 1986;27:145–152.

11. Eldred G, Miller GV, Stark WS, Feeney-Burns L. Lipofuscin: resolution of discrepant fluorescence data. *Science*. 1982;216:757–759.

12. Ng KP, Gugiu B, Renganathan K, et al. Retinal pigment epithelium lipofuscin proteomics. *Mol Cell Proteomics*. 2008;7:1397–1405.

13. Sparrow JR, Gregory-Roberts E, Yamamoto K, et al. The bisretinoids of retinal pigment epithelium. *Prog Retin Eye Res*. 2012;31:121–135.

14. Yamamoto K, Zhou J, Hunter JJ, Williams DR, Sparrow JR. Toward an understanding of bisretinoid autofluorescence bleaching and recovery. *Invest Ophthalmol Vis Sci*. 2012;53:3536–3544.

15. Dorey CK, Wu G, Ebenstein D, Garsd A, Weiter JJ. Cell loss in the aging retina. Relationship to lipofuscin accumulation and macular degeneration. *Invest Ophthalmol Vis Sci*. 1989;30:1691–1699.

16. Feeney-Burns L, Berman ER, Rothman H. Lipofuscin of human retinal pigment epithelium. *Am J Ophthalmol*. 1980;90:783–791.

17. Wing GL, Blanchard GC, Weiter JJ. The topography and age relationship of lipofuscin concentration in the retinal pigment epithelium. *Invest Ophthalmol Vis Sci*. 1978;17:601–607.

18. Østerberg GA. Topography of the layer of rods and cones in the human retina. *Acta Ophthalmol*. 1935;13:1–103.

19. Curcio CA, Sloan KR, Kalina RE, Hendrickson AE. Human photoreceptor topography. *J Comp Neurol*. 1990;292:497–523.

20. Boulton M, Marshall J. Repigmentation of human retinal pigment epithelial cells in vitro. *Exp Eye Res*. 1985;41:209–218.

21. Harman AM, Fleming PA, Hoskins RV, Moore SR. Development and aging of cell topography in the human retinal pigment epithelium. *Invest Ophthalmol Vis Sci*. 1997;38:2016–2026.

22. Del Priore LV, Kuo YH, Tezel TH. Age-related changes in human RPE cell density and apoptosis proportion in situ. *Invest Ophthalmol Vis Sci*. 2002;43:3312–3318.

23. Gao H, Hollyfield JG. Aging of the human retina. Differential loss of neurons and retinal pigment epithelial cells. *Invest Ophthalmol Vis Sci*. 1992;33:1–17.

24. Curcio CA, Millican CL, Allen KA, Kalina RE. Aging of the human photoreceptor mosaic: evidence for selective vulnerability of rods in central retina. *Invest Ophthalmol Vis Sci*. 1993;34:3278–3296.

25. Jackson GR, Owsley C, Curcio CA. Photoreceptor degeneration and dysfunction in aging and age-related maculopathy. *Ageing Res Rev*. 2002;1:381–396.

26. Curcio CA, Medeiros NE, Millican CL. The Alabama Age-Related Macular Degeneration Grading System for donor eyes. *Invest Ophthalmol Vis Sci*. 1998;39:1085–1096.

27. Gutierrez DB, Blakeley L, Goletz PW, et al. Mass spectrometry provides accurate and sensitive quantitation of A2E. *Photochem Photobiol Sci*. 2010;9:1513–1519.

28. McKechnie NM, Boulton M, Robey HL, Savage FJ, Grierson I. The cytoskeletal elements of human retinal pigment epithelium: in vitro and in vivo. *J Cell Sci*. 1988;91:303–312.

29. Snoddorly DM, Sandstrom MM, Leung IY, Zucker CL, Neuringer M. Retinal pigment epithelial cell distribution in central retina of rhesus monkeys. *Invest Ophthalmol Vis Sci*. 2002;43:2815–2818.

30. Delori FC, Goger DG, Dorey CK. Age-related accumulation and spatial distribution of lipofuscin in RPE of normal subjects. *Invest Ophthalmol Vis Sci*. 2001;42:1855–1866.

31. Duyckaerts C, Godefroy G. Voronoi tessellation to study the numerical density and the spatial distribution of neurones. *J Chem Neuroanat*. 2000;20:83–92.

32. Ooto S, Hangai M, Takayama K, et al. High-resolution imaging of the photoreceptor jayer in epiretinal membrane using adaptive optics scanning laser ophthalmoscopy. *Ophthalmology*. 2011;118:873–881.

33. Morgan JIW, Dubra A, Wolfe R, Merigan WH, Williams DR. In vivo autofluorescence imaging of the human and macaque retinal pigment epithelial cell mosaic. *Invest Ophthalmol Vis Sci*. 2009;50:1350–1359.

34. Delori F, Greenberg JP, Woods RL, et al. Quantitative measurements of autofluorescence with the scanning laser ophthalmoscope. *Invest Ophthalmol Vis Sci*. 2011;52:9379–9390.

35. Diggle PH, Liang PJ, Zeger KYSL. *Analysis of Longitudinal Data. SL Analysis of Longitudinal Data*. New York: Oxford University Press; 2002.

36. Hanley JA, Negassa A, Forrester JE. Statistical analysis of correlated data using generalized estimating equations: an orientation. *Am J Epidemiol*. 2003;157:364–375.

37. Curcio CA, Allen KA. Topography of ganglion cells in human retina. *J Comp Neurol*. 1990;300:5–25.

38. Panda-Jonas S, Jonas JB, Jakobczyk-Zmija M. Retinal pigment epithelial cell count, distribution, and correlations in normal human eyes. *Am J Ophthalmol*. 1996;121:181–189.

39. Ts'o MO, Friedman E. The retinal pigment epithelium. 3. Growth and development. *Arch Ophthalmol*. 1968;80:214–216.

40. Streeten BW. Development of the human retinal pigment epithelium and the posterior segment. *Arch Ophthalmol*. 1969;81:383–394.

41. Watzke RC, Soldevilla JD, Trune DR. Morphometric analysis of human retinal pigment epithelium: correlation with age and location. *Curr Eye Res*. 1993;12:133–142.

42. Burke JM, Hjelmeland LM. Mosaicism of the retinal pigment epitheliums. *Mol Interv*. 2005;5:9.

43. Lewis FT. The geometry of growth and cell division in epithelial mosaics. *Am J Bot*. 1943;30:766–776.

44. Ablonczy Z, Higbee D, Anderson DM, et al. Lack of correlation between the spatial distribution of A2E and lipofuscin fluorescence in the human retinal pigment epithelium. *Invest Ophthalmol Vis Sci*. 2013;54:5535–5542.

45. Greenberg JP, Duncker T, Woods RL, Smith RT, Sparrow JR, Delori FC. Quantitative fundus autofluorescence in healthy eyes. *Invest Ophthalmol Vis Sci*. 2013;54:5684–5693.

46. Schmidt SY, Peisch RD. Melanin concentration in normal human retinal pigment epithelium. Regional variation and age-related reduction. *Invest Ophthalmol Vis Sci*. 1986;27:1063–1067.

47. Curcio CA, Johnson M, Huang JD, Aging, Rudolf M. age-related macular degeneration, and the response-to-retention of apolipoprotein B-containing lipoproteins. *Prog Retin Eye Res*. 2009;28:393–422.

48. Cankova Z, Huang JD, Kruth HS, Johnson M. Passage of low-density lipoproteins through Bruch's membrane and choroid. *Exp Eye Res*. 2011;93:947–955.

49. Curcio CA, Owsley C, Jackson GR. Spare the rods, save the cones in aging and age-related maculopathy. *Invest Ophthalmol Vis Sci*. 2000;41:2015–2018.

50. Whitmore SS, Braun TA, Skeie JM, et al. Altered gene expression in dry age-related macular degeneration suggests early loss of choroidal endothelial cells. *Mol Vis*. 2013;19:2274–2297.

51. Ramrattan RS, van der Schaft TL, Mooy CM, de Bruijn WC, Mulder PG, de Jong PT. Morphometric analysis of Bruch's membrane, the choriocapillaris, and the choroid in aging. *Invest Ophthalmol Vis Sci*. 1994;35:2857–2864.

52. Birnbach CD, Jarvelainen M, Possin DE, Milam AH. Histopathology and immunocytochemistry of the neurosensory retina in fundus flavimaculatus. *Ophthalmology*. 1994;101:1211–1219.

53. Lewis FT. The effect of cell division on the shape and size of hexagonal cells. *Anat Rec*. 1926;33:331–355.

54. Kaldarar-Pedotti S. Mitotic activity of the pigment epithelium during embryonic and postembryonic development. *Adv Ophthalmol*. 1979;39:37–58.

55. Campisi J. d'Adda di Fagagna F. Cellular senescence: when bad things happen to good cells. *Nat Rev Mol Cell Biol*. 2007;8:729–740.

56. Ding JD, Johnson LV, Herrmann R, et al. Anti-amyloid therapy protects against retinal pigmented epithelium damage and vision loss in a model of age-related macular degeneration. *Proc Natl Acad Sci U S A*. 2011;108:E279–E287.

57. Katz ML. Potential role of retinal pigment epithelial lipofuscin accumulation in age-related macular degeneration. *Arch Gerontol Geriatr*. 2002;34:359–370.

58. Gray DA, Woulfe J. Lipofuscin and aging: a matter of toxic waste. *Sci Aging Knowledge Environ*. 2005;2005:re1.

59. Katz ML, Robison WG. What is lipofuscin? Defining characteristics and differentiation from other autofluorescent lysosomal storage bodies. *Arch Gerontol Geriatr*. 2002;34:169–184.

60. Eldred G. Age pigment structure. *Nature*. 1993;364:396.

61. Sparrow JR, Wu Y, Kim CY, Zhou J. Phospholipid meets all-trans-retinal: the making of RPE bisretinoids. *J Lipid Res*. 2010;51:247–261.

62. Sparrow JR, Dowling JE, Bok D, Understanding RPE. Lipofuscin. *Invest Ophthalmol Vis Sci*. 2013;54:8325–8326.

63. Holz FG, Bellman C, Staudt S, Schutt F, Volcker HE. Fundus autofluorescence and development of geographic atrophy in age-related macular degeneration. *Invest Ophthalmol Vis Sci*. 2001;42:1051–1056.

64. Julien S, Schraermeyer U. Lipofuscin can be eliminated from the retinal pigment epithelium of monkeys. *Neurobiol Aging*. 2012;33:2390–2397.

65. Meleth AD, Wong WT, Chew EY. Treatment for atrophic macular degeneration. *Curr Opin Ophthalmol*. 2011;22:190–193.

66. Kubota R, Boman NL, David R, Mallikaarjun S, Patil S, Birch D. Safety and effect on rod function of ACU-4429, a novel small-molecule visual cycle modulator. *Retina*. 2012;32:183–188.

67. Nociari MM, Lehmann GL, Perez Bay AE, et al. Beta cyclodextrins bind, stabilize, and remove lipofuscin bisretinoids from retinal pigment epithelium. *Proc Natl Acad Sci U S A*. 2014;111:E1402–E1408.

68. Evans JB, Syed BA. New hope for dry AMD? *Nat Rev Drug Discov*. 2013;12:501–502.

69. Mainster MA, Turner PL. Blue-blocking IOLS vs. short-wavelength visible light: hypothesis-based vs. evidence-based medical practice. *Ophthalmology*. 2011;118:1–2.

70. Carson D, Margrain TH, Patel A. New approach to evaluate retinal protection by intraocular lenses against age-related lipofuscin accumulation-mediated retinal phototoxicity. *J Cataract Refract Surg*. 2008;34:1785–1792.

71. Hwang JC, Chan JW, Chang S, Smith RT. Predictive value of fundus autofluorescence for development of geographic atrophy in age-related macular degeneration. *Invest Ophthalmol Vis Sci*. 2006;47:2655–2661.

72. Rudolf M, Vogt SD, Curcio CA, et al. Histologic basis of variations in retinal pigment epithelium autofluorescence in eyes with geographic atrophy. *Ophthalmology*. 2013;120:821–828.

73. Bhosale P, Serban B, Bernstein PS. Retinal carotenoids can attenuate formation of A2E in the retinal pigment epithelium. *Arch Biochem Biophys*. 2009;483:175–181.

74. Grey AC, Crouch RK, Koutalos Y, Schey KL, Ablonczy Z. Spatial localization of A2E in the retinal pigment epithelium. *Invest Ophthalmol Vis Sci*. 2011;52:3926–3933.

75. Kim JY, Zhao H, Martinez J, et al. Noncanonical autophagy promotes the visual cycle. *Cell*. 2013;154:365–376.

76. Tarallo V, Hirano Y, Gelfand BD, et al. DICER1 loss and Alu RNA induce age-related macular degeneration via the NLRP3 inflammasome and MyD88. *Cell*. 2012;149:847–859.

77. Pikuleva IA, Curcio CA. Cholesterol in the retina: the best is yet to come. *Prog Retin Eye Res*. 2014;41C:64–89.

78. Mrejen S, Sato T, Curcio CA, Spaide RF. Assessing the cone photoreceptor mosaic in eyes with pseudodrusen and soft Drusen in vivo using adaptive optics imaging. *Ophthalmology*. 2014;121:545–551.

79. Jackson GR, Scott IU, Kim IK, Quillen DA, Iannaccone A, Edwards JG. Diagnostic sensitivity and specificity of dark adaptometry for detection of age-related macular degeneration. *Invest Ophthalmol Vis Sci*. 2014;55:1427–1431.

80. Rossi EA, Rangel-Fonseca P, Parkins K, et al. In vivo imaging of retinal pigment epithelium cells in age related macular degeneration. *Biomed Opt Express*. 2013;4:2527–2539.

81. Scoles D, Sulai YN, Dubra A. In vivo dark-field imaging of the retinal pigment epithelium cell mosaic. *Biomed Opt Express*. 2013;4:1710–1723.

82. Fawzi AA, Lee N, Acton JH, Laine AF, Smith RT. Recovery of macular pigment spectrum in vivo using hyperspectral image analysis. *J Biomed Opt*. 2011;16:106008.

83. Duncker T, Greenberg JP, Sparrow JR, Smith RT, Quigley HA, Delori FC. Visualization of the optic fissure in short-wavelength autofluorescence images of the fundus. *Invest Ophthalmol Vis Sci*. 2012;53:6682–6686.

84. Moore DJ, Hussain AA, Marshall J. Age-related variation in the hydraulic conductivity of Bruch's membrane. *Invest Ophthalmol Vis Sci*. 1995;36:1290–1297.

85. Curcio CA, Messinger JD, Sloan KR, McGwin G, Medeiros NE, Spaide RF. Subretinal drusenoid deposits in non-neovascular age-related macular degeneration: morphology, prevalence, topography, and biogenesis model. *Retina*. 2013;33:265–276.